energies

MDPI

Article

Performance Comparison and Optimization of a PMSM Based on Hybrid-Type Permanent Magnet with Two Kinds of Rotor Topology

Kai Yang, Lu Zhang *, Mengyao Wang and Chunyu Du

Department of Electrical Engineering and Automation, Harbin Institute of Technology, Harbin 150080, China; 18903603938@163.com (K.Y.); wangmy@stu.hit.edu.cn (M.W.); 22s106142@stu.hit.edu.cn (C.D.)
* Correspondence: zhanglu24@hit.edu.cn

Abstract: This study focuses on designing and optimizing Permanent Magnet Synchronous Motors (PMSMs) using hybrid rare earth and ferrite materials. Two distinctive rotor topologies of the Hybrid-Type Permanent Magnet Motor (HTPMM) are proposed: series and parallel magnetic circuits. Initially, the rotor topology and magnetic circuit principles of both the prototype and the designed HTPMM are introduced. Subsequently, a multi-objective genetic algorithm is employed to optimize the two HTPMMs, determining the final optimized parameters. Thise study further analyzes the cost advantage of HTPMMs from the perspective of permanent magnet materials, and detailed finite element analysis is conducted to evaluate the electromagnetic performance, including the air-gap flux density, no-load back electromotive force, cogging torque, load torque characteristics, and demagnetization properties. A comparative analysis of the prototype and two designed motors reveals that the HTPMM exhibits similar performance to the prototype, effectively reducing the usage of rare earth materials and significantly lowering the manufacturing costs. This research validates the feasibility of reducing rare earth material usage while maintaining a similar performance and provides a new perspective for the design of permanent magnet motors.

Keywords: PMSM; hybrid permanent magnet materials; magnetic circuit structure; performance comparison; optimization

Citation: Yang, K.; Zhang, L.; Wang, M.; Du, C. Performance Comparison and Optimization of a PMSM Based on Hybrid-Type Permanent Magnet with Two Kinds of Rotor Topology. *Energies* **2024**, *17*, 557. https://doi.org/10.3390/en17030557

Academic Editor: Daniel Morinigo-Sotelo

Received: 20 December 2023
Revised: 16 January 2024
Accepted: 22 January 2024
Published: 23 January 2024

1. Introduction

As society progresses economically and socially, the concerns about environmental issues and the scarcity of energy resources continue to grow. Permanent Magnet Synchronous Motors (PMSMs) have been widely adopted in various fields due to their high power density and efficiency [1]. Continuously, new schemes for PMSMs have been proposed to enhance their performance [2,3]. Among these, Interior Permanent Magnet Synchronous Motors (IPMSMs) have gained favor due to their broad Constant Power Speed Range [4]. However, fluctuations in the supply and price of rare earth permanent magnet materials, such as NdFeB and SmCo, have restricted their applications. According to the data from the U.S. Department of Energy, rare earth magnets constitute 20% to 30% of the total motor cost [5]. Hence, the recent escalation in rare earth permanent magnet material prices has prompted widespread efforts aimed at reducing their usage in permanent magnet machines while maintaining the same level of performance. Additionally, as the temperatures rise, the demagnetization resistance of rare earth permanent magnet materials diminishes, potentially leading to localized demagnetization under extreme operating conditions [6,7].

When addressing the utilization of rare earth materials and performance enhancement in permanent magnet motors, there are four primary solutions or paradigms in motor design. These paradigms range from the complete exclusion of rare earth materials to various design structures based on ferrites and the mixed usage of rare earth and ferrite materials. Here is a brief overview of these four primary design schemes for permanent magnet motors:

1. The motor topologies are devoid of permanent magnet materials; some examples include synchronous reluctance motors, switched reluctance motors, and induction motors, which do not utilize permanent magnet materials. However, they often encounter issues related to efficiency and torque density, leading to higher operational costs;
2. Permanent magnet designs based on ferrites: This design aims to entirely replace rare earth permanent magnet materials, employing ferrites as the permanent magnet material. Nevertheless, ferrite magnets have certain design limitations, such as low residual magnetism and irreversible demagnetization phenomena [8,9], restricting their competitive performance;
3. Hybrid permanent magnet motor topologies: This design incorporates both ferrite and rare earth permanent magnet materials, partially substituting rare earth permanent magnet materials to reduce the manufacturing costs. This hybrid design maintains an acceptable torque capability, while offering an economically viable choice for the manufacturers [10];
4. Permanent magnet motor topologies based on rare earth permanent magnet materials: This design relies entirely on high-energy rare earth permanent magnet materials, modifying the motor's magnetic structure to reduce the usage of rare earth permanent magnet materials. Such attempts aim to reduce the costs while maintaining the performance, but this design might potentially increase the manufacturing expenses.

There are primarily three types of magnet arrangements for hybrid permanent magnet motors: series, parallel, and hybrid structures [11]. In a parallel structure, the magnetic fluxes of two types of permanent magnets do not intersect with each other, and the magnetic reluctance of only one type of permanent magnet exists in a magnetic circuit [12]. Hence, parallel mixed magnetic material motors are superior in performance to the series types. However, due to the low coercive force of ferrite materials, ferrites are prone to demagnetization [13]. In contrast, in a series structure, the higher magnetic reluctance in the magnetic circuit results in less magnetic flux produced for the same magnetic field intensity, leading to a worse electromagnetic performance. Replacing highly coercive rare earth permanent magnet materials with poorly coercive ferrite materials might lead to a decline in the output. To enhance the demagnetization resistance of ferrites in the parallel structure, the authors of reference [14] utilize a magnetic flux barrier to regulate the magnetic flux path and reduce the risk of the demagnetization of ferrites. The existing research has been conducted to improve the rotor optimization to enhance the output torque of parallel hybrid permanent magnet motors. Based on the symmetric rotor hybrid magnetic pole PMSM, the concept of an asymmetric rotor hybrid magnetic pole PMSM has been proposed [15]. In this design, the radial arrangement of the ferrite permanent magnet remains unchanged, while its centerline rotates an angle α relative to the q-axis, thereby improving the reluctance torque.

The stator structure of hybrid magnetic pole PMSMs has also undergone improvements in other studies [16]. In this research, both ferrite and NdFeB are utilized as magnetic sources, with four small NdFeB pieces installed on specific rotor teeth. To maximize the utilization of the stator yoke space and provide more magnetic field strength, ferrites are intentionally embedded into the stator yoke. Due to the distinctive magnetization directions of the two permanent magnet materials, a concentrated magnetic flux effect has been achieved, offering a relatively higher torque output capability. The authors of reference [17] designed two different structures of hybrid permanent magnet motors with

parallel and series magnetic circuits, finding that the former requires less rare earth permanent magnet material to achieve the torque requirements, whereas latter requires more rare earth permanent magnet material but exhibits a lower cogging torque. Due to the performance differences between rare earth and ferrite permanent magnet materials, both the motors exhibit a lower Total Harmonic Distortion (THD) when excessively wound. The authors of reference [18,19] proposed a U-shaped IPMSM design, where the hybrid magnetic pole ferrite permanent magnet is positioned centrally. The rotor of this design, after optimization, aims to provide more reluctance torque, while reducing the usage of rare earth permanent magnet materials without compromising the electromagnetic torque. Additionally, other researchers haves analyzed two hybrid magnetic pole schemes, namely, double-layer and radial structures, investigating the electromagnetic characteristics such as the electromagnetic torque, flux-weakening ability, and demagnetization risk to verify the superiority of low-cost IPMSMs [20].

The authors or reference [21] introduced a spoke-type hybrid magnetic motor and compared it with a pure rare earth motor. The results indicated that due to the extensive use of ferrite materials and the specific magnetism-polarizing effect of the spoke-type structure, the output torque closely resembled that of the pure rare earth material motor. However, the increased rotor mass due to the large amount of ferrite used led to heightened mechanical stress on the rotor at high speeds [22]. Additionally, the reluctance torque of the spoke-type Permanent Magnet Synchronous Motor is low, making it unsuitable for high-speed applications.

In the face of the ongoing challenges posed by the escalating global prices for rare earth materials, this paper presents an innovative solution to propel the development of Hybrid-Type Permanent Magnet Motor (HTPMM). Firstly, the introduction of ferrites as a substitution for some NdFeB achieves a balance between sustainability and economic efficiency in material selection. Secondly, the groundbreaking design of both series and parallel magnetic circuit rotor structures marks a significant advancement in motor architecture. In terms of motor optimization, a multi-objective genetic algorithm is employed to ensure the motor is optimized across various performance indicators, while maintaining a minimum output torque equivalent to that of the prototype. Lastly, through a comprehensive performance comparison, the newly proposed HTPMM exhibits a performance comparable to, if not superior to, the traditional prototype. This offers a viable and efficient solution to address the challenges posed by the rise in rare earth prices. These innovations represent the focus of this study, providing substantial impetus for the advancement of HTPMM.

This study focuses on HTPMMs. We will propose two HTPMMs with distinct rotor topological structures for analysis and comparison. In the following sections, we will introduce the topology and specifications of these two HTPMMs. Our analysis will delve into the magnetic flux paths and equivalent magnetic circuits of these HTPMMs to illustrate the disparities arising from different rotor topological structures. Subsequently, in the next section, a multi-objective genetic algorithm will be employed for motor optimization, ensuring that the motor parameters are determined under the condition that the motor performance is not inferior to the prototype. Additionally, we will compare the usage costs of permanent magnets in the three types of motors and analyze the cost advantages of the HTPMM over the traditional pure rare earth motors. Following this, the comprehensive performance analysis of these two HTPMMs will be presented, providing detailed comparisons of the three motors in terms of the no-load back electromotive force, and air-gap magnetic density, output torque, and demagnetization of permanent magnets. Finally, the final section will present the overall conclusions of this study.

2. Rotor Topologies and Magnetic Circuit Principles

2.1. Prototype

The motor depicted in Figure 1a,b serves as the prototype for this study, utilizing a singular NdFeB permanent magnet material. The NdFeB magnets arranged in a V-shaped configuration at each pole effectively enhance the air-gap flux density waveform, thereby reducing the back electromotive force harmonics. Figure 1c illustrates the equivalent magnetic circuit of this motor, where F_{RE} represents the magnetic potential of NdFeB, R_{RE} denotes the magnetic reluctance of NdFeB, and R_g signifies the air-gap reluctance. The motor specifications, as presented in Table 1, indicate a rated current of 5 A and a rated speed of 1000 rpm. Notably, applying an effective phase current of 5 A to the motor windings results in an average torque output of 5 N.

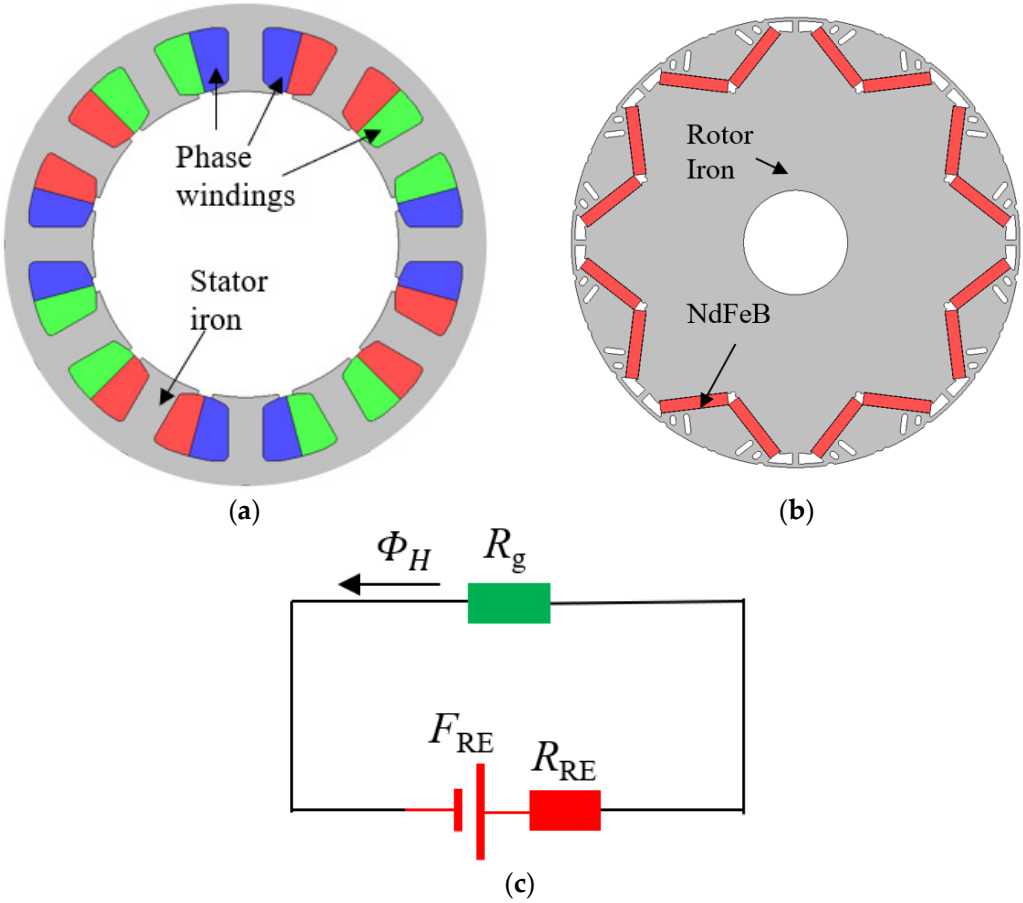

Figure 1. Prototype motor: (**a**) stator; (**b**) rotor; (**c**) equivalent magnetic circuit.

Table 1. Prototype motor parameters.

Parameters	Values	Parameters	Values
Rated speed (r/min)	1000.0	Rated current (A)	5.0
Rated torque (N·m)	4.8	Stack length (mm)	35.0
Airgap length (mm)	0.5	Stator outer diameter (mm)	47.0
NdFeB volume (cm^3)	7.0	Rotor outer diameter(mm)	27.75
Rotor inner diameter (mm)	6.5	Turns per slot	76.0

2.2. HTPMM

This paper introduces a novel type of HTPMM, which generates an excitation magnetic field by combining rare earth and ferrite permanent magnet materials. Based on the different placements of the two types of permanent magnets, this motor proposes series magnetic circuit (SMC) and parallel magnetic circuit (PMC) permanent magnet motors: PMC-HTPMM and SMC-HTPMM, respectively. For comparative purposes, the newly proposed motor maintains the stator of the prototype, with the stator's outer diameter, inner diameter, and coil turns identical to those of the prototype.

Figure 2a,b, respectively, illustrate the topological structures of the PMC-HTPMM and the SMC-HTPMM. As depicted in Figure 2a, it is observable that the NdFeB and ferrite in the PMC-HTPMM are radially positioned along the motor rotor, with their axes aligned. This configuration magnetizes both types of permanent magnets tangentially, termed a spoke-type structure. Such a structure significantly enhances the air-gap flux density of the motor, meaning it achieves a similar output torque using fewer permanent magnets compared to the traditional motors. However, this structure has notable drawbacks: the radial placement of the permanent magnets generates a substantial leakage flux, potentially deteriorating the output performance if not meticulously designed. Moreover, this structure induces more harmonic components in the air-gap flux, impacting the sinusoidal nature of the back electromotive force and resulting in an increased torque ripple, significantly hindering the suppression of electromagnetic noise. In this study, an effectively designed magnetic circuit is employed to reduce the rotor leakage flux, while the addition of isolation holes substantially enhances the air-gap flux density waveform of the motor. Due to the minimal residual magnetism of ferrite, which is only one-third of the size of that of NdFeB, achieving a similar electromagnetic performance as the prototype motor necessitates the addition of some NdFeB with a higher residual magnetism to augment the air-gap flux density. In this study, an asymmetric rotor structure composed of V-shaped permanent magnets made of NdFeB was added to the spoke-type rotor composed of ferrite at each N pole, constituting the SMC-HTPMM. This asymmetric rotor structure profoundly impacts motor performance, generating numerous odd-harmonic components. To mitigate these harmonics, a multi-objective genetic algorithm was employed to optimize the motor by adjusting the angle between the adjacent radially positioned ferrite and optimizing the dimensions of the permanent magnets. This optimization resulted in a performance that was similar to the prototype motor.

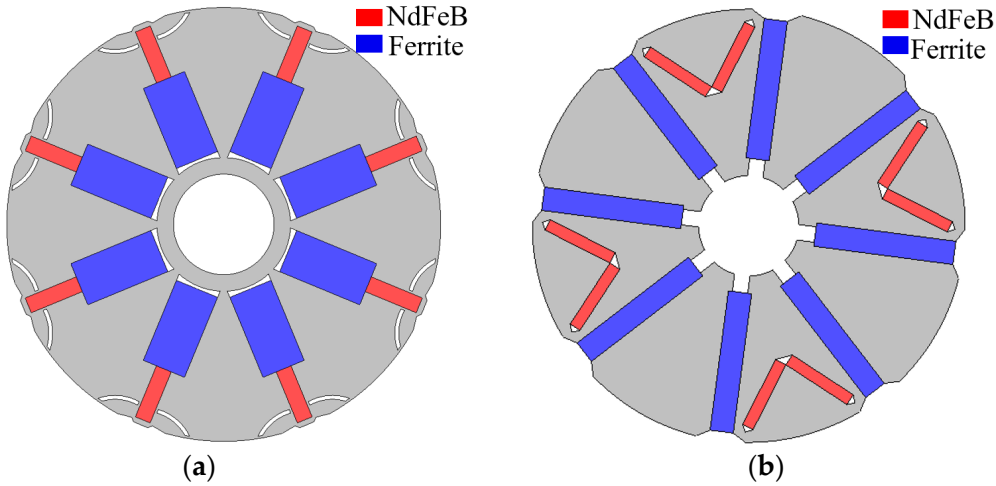

Figure 2. Rotor Topological Structures: (**a**) Parallel; **(b)** Series.

Figure 3a,b depict the equivalent magnetic circuit diagrams of the parallel magnetic circuit Hybrid-Type Permanent Magnet Motor (PMC-HTPMM) and the series magnetic circuit Hybrid-Type Permanent Magnet Motor (SMC-HTPMM), respectively. In the PMC-HTPMM, each type of permanent magnet only carries its self-generated magnetic flux, displayed in parallel connection within the equivalent magnetic circuit diagram. In the SMC-HTPMM, the magnetic flux produced by both types of permanent magnet materials circulates between them, which is illustrated in series within the equivalent magnetic circuit diagram. FFE and FRE denote the magnetic potential of the ferrite permanent magnet and the NdFeB permanent magnet, respectively. RFE and RRE represent the magnetic reluctance of the ferrite permanent magnet and the NdFeB permanent magnet, while *R*g signifies the magnetic reluctance of the air gap. The equivalent magnetic circuit assumes the neglect of leakage flux. The parameters in the equivalent magnetic circuit adhere to Kirchhoff's law for magnetic circuits.

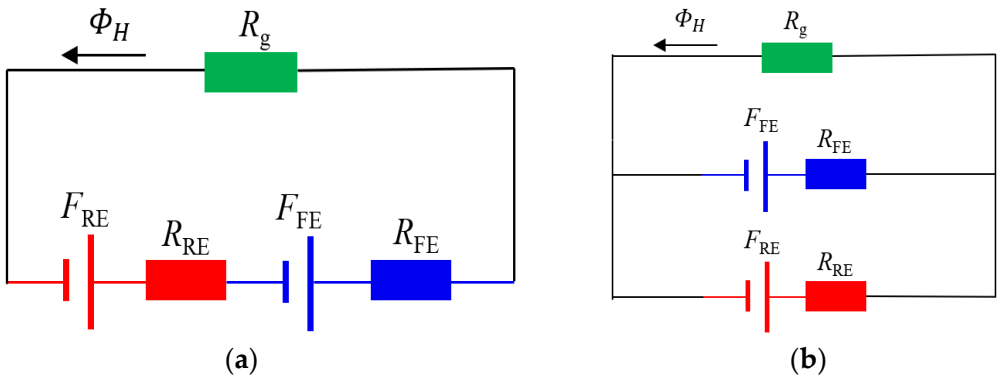

Figure 3. Equivalent magnetic circuit: (**a**) parallel; (**b**) series.

3. Optimization of Parallel Magnetic Circuit (PMC) and Series Magnetic Circuit (SMC) Motors

To obtain the magnetic field distribution within the motor, there are three commonly employed methods including analytical, magnetic circuit, and the widely utilized finite element method. With the rapid advancements in computer technology, the finite element method has become the predominant approach for simulating motors magnetic fields. In this study, JMAG 22.1.01 software is utilized for finite element simulation and optimization of the magnetic field distribution.

3.1. Multi-Objective Optimization Workflow

In the realm of electric motor design, the application of multi-objective genetic algorithms has proven instrumental in concurrently optimizing many different performance objectives. With the considerations ranging from efficiency improvement to cost reduction and increased power output, the inherent complexities necessitate a holistic approach. Multi-objective genetic algorithms, adept at navigating such intricacies, offer an efficient means of achieving a well-balanced electric motor design.

The optimization process unfolds through the clear definition of performance objectives, parameter encoding, and the formulation of a comprehensive fitness function. The evolutionary steps, marked by the random initialization of design solutions and iterative refinement via genetic algorithm operations, culminate in a Pareto front representing optimal designs that achieve multiple objectives. To illustrate this process, a schematic depiction of the electric motor optimization workflow, encapsulating these key stages, is presented in Figure 4.

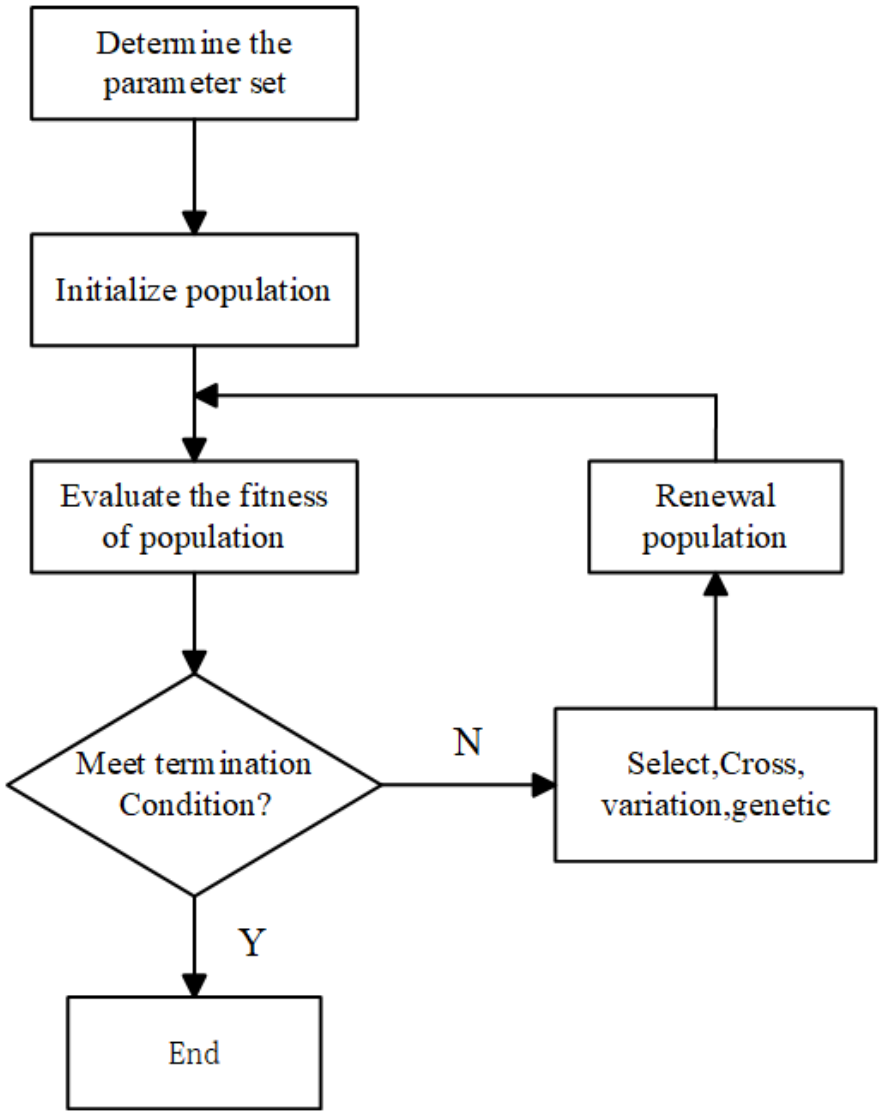

Figure 4. Process of the applied genetic algorithm.

In this study, the optimization of the motor is executed through the utilization of the optimization module using JMAG, integrating some efficient optimization algorithms. The key steps involved in this process are outlined as follows:

Firstly, the objective function is defined with the primary goal of maximizing the motor's output torque relative to the initial motor torque. Simultaneously, the objective function addresses this imperative to keep the torque ripple below 20%. The constraint conditions are then specified to ensure that the optimized motor aligns with the practical application requirements. One such condition involves maintaining the sum of the lengths of ferrite and NdFeB at 18.4. The selection of input parameters crucial for motor optimization include w_1, w_2, r_{out}, h_1, h_2, and r_{in}. The optimization process proceeds iteratively using JMAG, wherein the input parameters are adjusted to optimize the defined objective function. Each iteration involves adjusting the motor's design parameters based on feedback from the objective function and constraint conditions.

To enhance the clarity, a concise graphical representation of the motor optimization process is presented in Figure 5, providing a visual overview of the iterative steps for achieving an optimal motor performance.

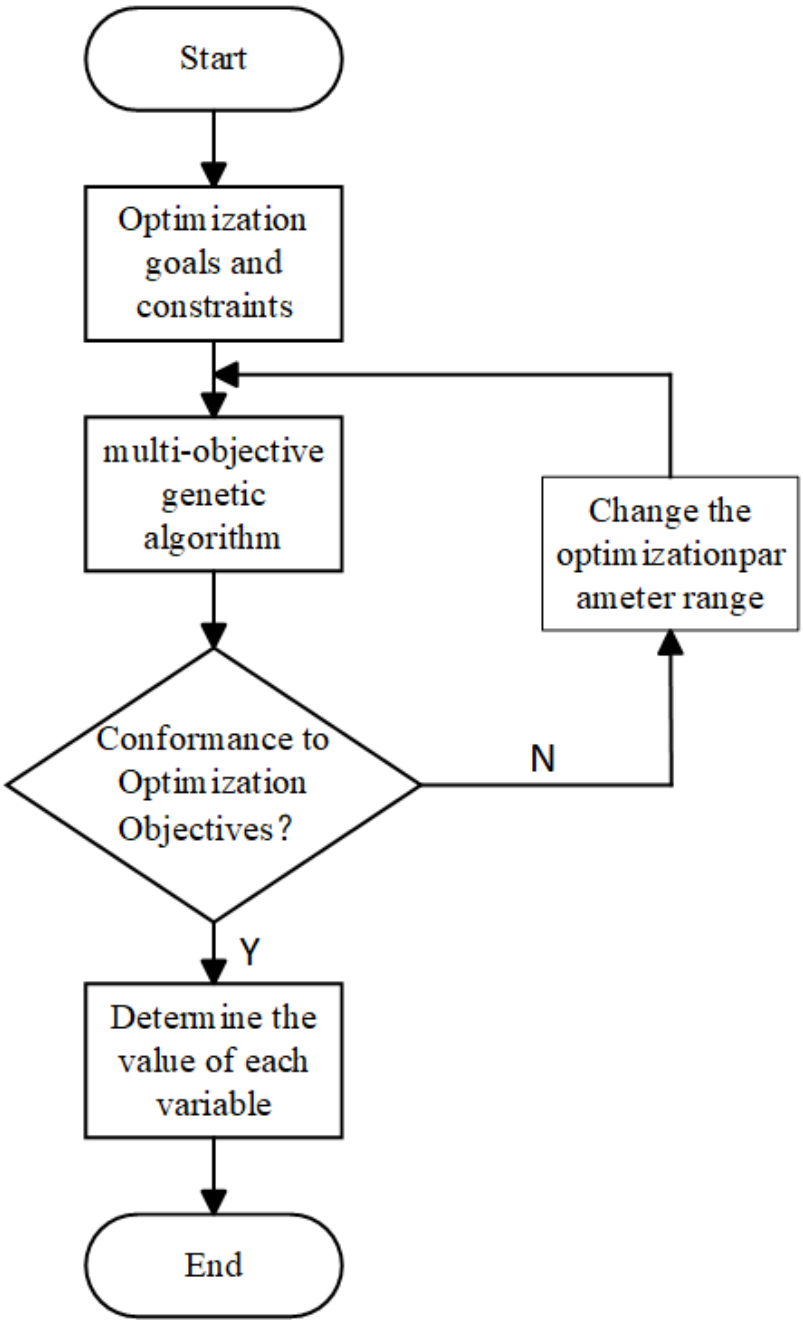

Figure 5. Optimization process.

3.2. PMC-HTPMM

As previously mentioned, in the PMC-HTPMM, both ferrite and NdFeB are radially positioned, using rectangular shapes to represent both the materials, with their axes aligned. The spoke-type rotor topology incorporates appropriately designed separating holes to reduce the leakage flux, Which can be significant. To acquire ideal motor output data, the preliminary determination of the dimensions of the ferrite and NdFeB is necessary. Subsequently, finite element analysis software is employed for the parameterized modeling of the motor. Genetic algorithms are then applied for multi-objective optimization design of multiple parameters, resulting in the required dimensions. The spoke-type rotor generates a considerable harmonic air-gap flux, significantly affecting the sinusoidal behavior of the back electromotive force (EMF). In this design, unique arc-shaped separating holes have

been used, markedly improving the air gap flux waveform, and substantially reducing the torque ripple in the motor.

Figure 6 illustrates the parameters involved in multi-objective optimization. Specifically, w_1 and w_2 represent the widths of ferrite and NdFeB, respectively, while h_1 and h_2 represent their respective lengths. Additionally, the parameters introduced are the inner r_{in} and outer circular rad r_{out} of the inter-magnet hole. Throughout optimization, the combined lengths of ferrite and NdFeB, represented by h_1 and h_2, respectively, were constrained to 18.4. The area of NdFeB was consistently set at 14 mm^2. To explore the influence of variations in w_1 and w_2 on the motor's output performance, an investigation was conducted. Figure 7 presents the changes in the motor's average output torque as w_1 and w_2 vary under an effective current input of 5 A. Remarkably, it is evident that the average torque shows an ascending trend with the increase in w_2. However, as w_1 gradually increases, the output torque initially rises, followed by a subsequent decrement.

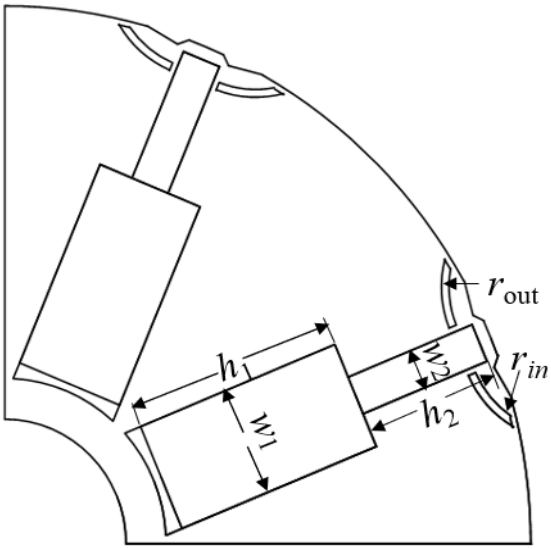

Figure 6. Parameterized design of the rotor for PMC-HTPMM.

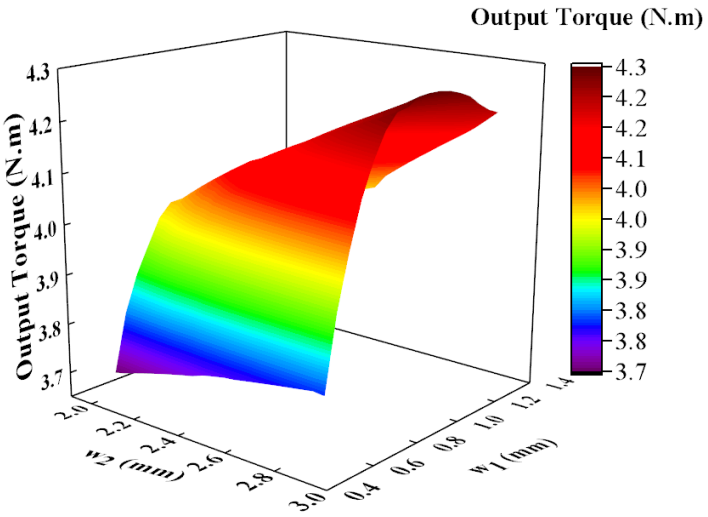

Figure 7. Output torque variation with parameters w_1 and w_2.

Commencing the optimization process for the PMC-HTPMM, we initially define the objective function, aiming to maximize the motor's output torque in relation to its initial torque while concurrently ensuring that the torque ripple remains below 20%. The constraints are then meticulously outlined to guarantee the optimized motor aligns with

practical application requirements, notably maintaining the sum of the ferrite and NdFeB lengths at 18.4. Referring to the initial parameters outlined in Table 2 and the optimization range specified in Table 3 for the SMC-HTPMM, the crucial input parameters, including w_1, w_2, r_{out}, h_1, h_2, and r_{in}, are systematically selected.

Table 2. Initial parameters of PMC-HTPMM.

Parameters	Values	Parameters	Values
w_1 (mm)	4	h_1 (mm)	12
w_2 (mm)	3	h_2 (mm)	4
r_{out} (mm)	8	r_{in} (mm)	6

Table 3. Optimization range of PMC-HTPMM.

Parameters	Optimization Range	Parameters	Optimization Range
w_1 (mm)	3–6	h_1 (mm)	9–13
w_2 (mm)	$14/h_2$	h_2 (mm)	18.4–h_1
r_{out} (mm)	4.2–9	r_{in} (mm)	4–9

Iterative optimization is performed using JMAG, dynamically adjusting the input parameters to optimize the predefined objective function. Each iteration adapts the motor's design parameters based on continuous feedback from both the objective function and the established constraint conditions. This structured approach ensures a systematic exploration of the optimization landscape, ultimately refining the PMC-HTPMM design for enhanced performance.

Figure 8 depicts the variation in the motor's torque ripple concerning the changes in w_1 and w_2. It is evident from the graph that w_2 has a minimal impact on the motor's torque ripple. However, the magnitude of w_1 significantly influences the torque ripple, showing a decreasing trend as w_1 increases. This suggests that the dimensions of NdFeB notably affect the motor output performance. Figure 9 illustrates the optimization results, revealing that a substantial portion in the bottom-right corner meets the motor design requirements. It is essential to strike a balance between the average torque value and torque ripple rate when selecting the optimal parameters. The final parameters, as depicted in Table 4, serve as a refined configuration that satisfies both the design criteria, enhancing the overall performance of the motor.

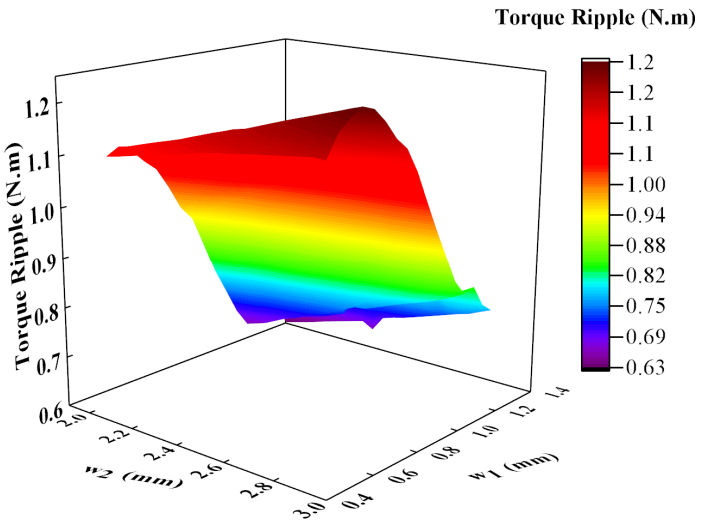

Figure 8. Torque ripple with variation parameters w_1 and w_2.

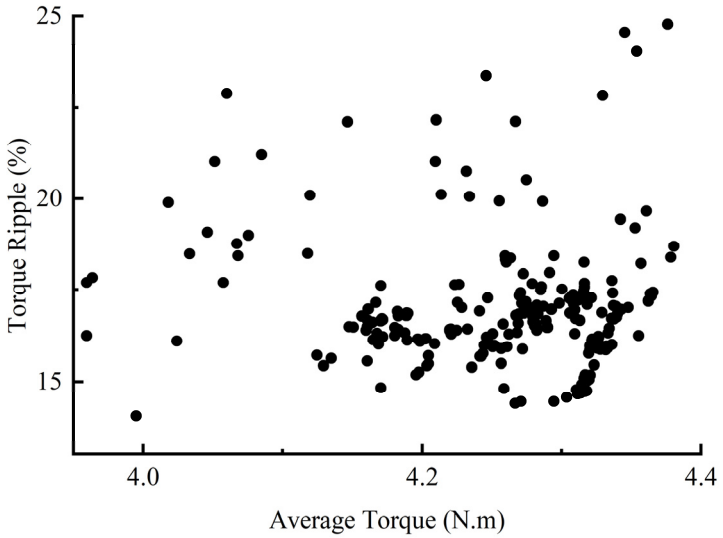

Figure 9. Optimization results of PMC-HTPMM.

Table 4. Final design parameters for PMC-HPMM motor.

Parameters	Values	Parameters	Values
w_1 (mm)	6.0	h_1 (mm)	14.0
w_2 (mm)	3.1	h_2 (mm)	4.4
r_{in} (mm)	4.3	r_{out} (mm)	4.7
NdFeB volume (cm^3)	3.8	Ferrite volume (cm^3)	2.3

3.3. SMC-HTPMM

The newly proposed series hybrid permanent magnet motor's topology is based on the spoke-type rotor composed of ferrite. In addition to ferrite, a pair of NdFeB V-shaped permanent magnets are added at each N pole. This structure significantly enhances the air-gap magnetic field density. However, this asymmetric structure causes substantial air-gap magnetic flux density distortion. Therefore, optimizing the rotor topology is necessary. In this study, optimization involves not only the dimensions and placement positions of the two types of magnetic steel, but also the parameterized analysis of the angle between the adjacent, radially placed ferrites. The motor optimization parameters are shown in Figure 10.

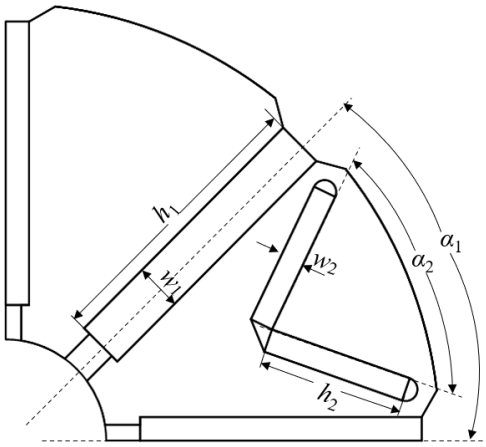

Figure 10. Parameterized design of the rotor for SMC-HTPMM.

In Figure 10, the multi-objective optimization parameters for the series magnetic circuit are presented. The respective widths of ferrite and NdFeB, represented by w_1 and w_2, and the respective lengths of ferrite and NdFeB, denoted as h_1 and h_2, are crucial aspects of this unique asymmetric structure. To optimize this configuration, the angles between the adjacent permanent magnets must be considered, with α_1 and α_2 signifying the angles between ferrite and NdFeB, respectively. The optimization process adheres to the initial parameters outlined in Table 5 and follows the specified optimization range detailed in Table 6 for the SMC-HTPMM. This ensures a comprehensive exploration within defined bounds to achieve an optimized series magnetic circuit configuration.

Table 5. Initial parameters of SMC-HTPMM.

Parameters	Values	Parameters	Values
w_1 (mm)	3	h_1 (mm)	18
w_2 (mm)	2.6	h_2 (mm)	8.7
NdFeB volume (cm^3)	3.9	Ferrite volume (cm^3)	7.84
α_1 (°)	45.5	α_2 (°)	79.5

Table 6. Optimization range of SMC-HTPMM.

Parameters	Optimization Range	Parameters	Optimization Range
w_1 (mm)	3–6	h_1 (mm)	18
w_2 (mm)	1.5–2.5	h_2 (mm)	$14/w_2$
α_1 (°)	44–50	α_2 (°)	60–85

The harmonics in the no-load back EMF is a significant factor causing torque ripples in the motor. THD is introduced here to characterize the sinusoidal Ty of the no-load back EMF. Figure 11 illustrates the variation in the THD and cogging torque peak-to-peak value of the motor at 1000 r/min with the angle α_1. It is observed that they both exhibit similar trends. In contrast to the conventional motors, in the SMC-HTPMM, when α_1 is 50°, both the THD and cogging torque reach their minimum values. The minimum THD is 5.5%, and the minimum cogging torque peak-to-peak value is 0.15 N.m. This verifies the substantial impact of THD of the no-load back EMF on the cogging torque; a smaller THD corresponds to a smaller cogging torque in the motor. Figure 12 presents the final optimization results.

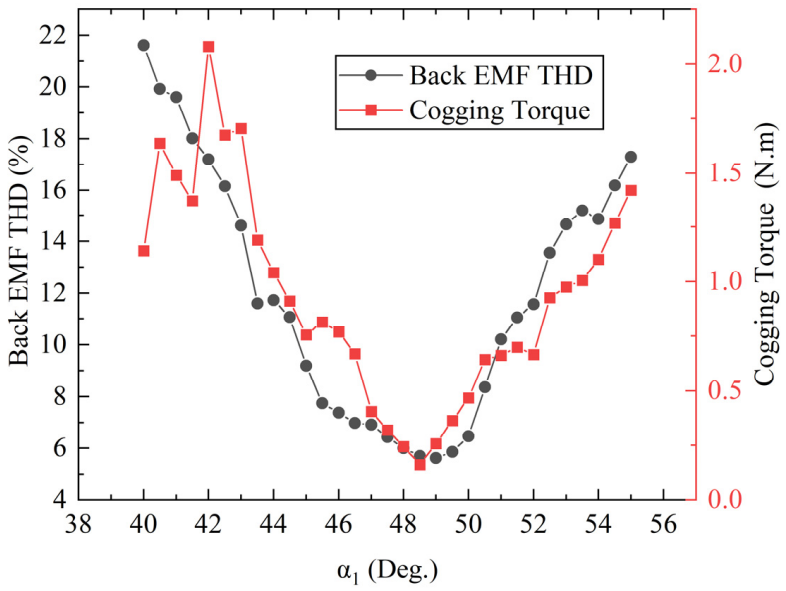

Figure 11. Variation curves of back EMF THD and cogging torque with α_1.

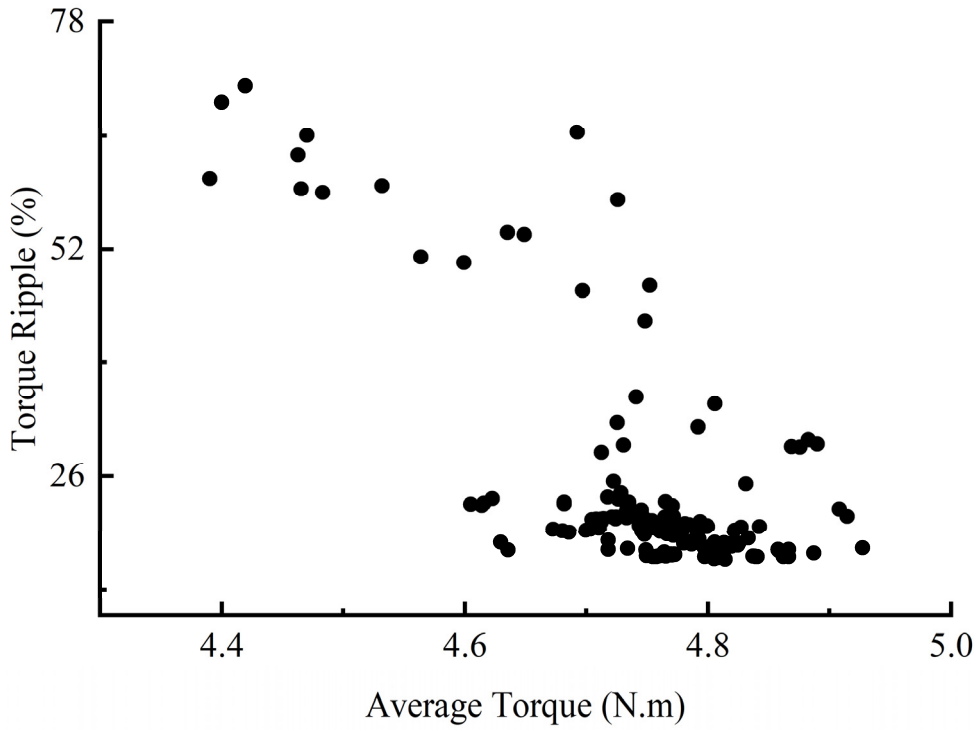

Figure 12. Optimization results of SMC-HTPMM.

For the ease of comparison, both the PMC-HTPMM and SMC-HTPMM utilized the same quantity of NdFeB. Figure 12 presents the optimization results for the SMC-HTPMM, with the bottom-right corner displaying the available choices. Similar to the optimization process for the PMC-HTPMM, a comprehensive consideration of both the motor's average torque value and torque ripple rate is crucial. The final motor parameters are detailed in Table 7, reflecting a judicious selection that balances these key performance criteria.

Table 7. Final design parameters for SMC-HPMM motor.

Parameters	Values	Parameters	Values
w_1 (mm)	5.8	h_1 (mm)	18.0
w_2 (mm)	1.5	h_2 (mm)	8.9
NdFeB volume (cm^3)	3.9	Ferrite volume (cm^3)	29.2
α_1 (°)	50.0	α_2 (°)	84.5

3.4. Cost Analysis

Due to the sharp rise in the prices of rare earth materials, and thus permanent magnet materials, currently, NdFeB is the most commonly used material in permanent magnet motors. However, its high cost has been a limiting factor for the industrial development of permanent magnet motors. Presently, the cost of NdFeB is USD 83.0 per kilogram, which is several times higher than that of ferrite. The price of ferrite materials remains at USD 5 per kilogram. As NdFeB has a density of 7500 kg/m^3 and ferrite has a density of 5000 kg/m^3, the cost of the permanent magnet materials for each type of motor is calculated as the product of volume, density, and unit price.

Table 8 below presents a cost comparison between the newly proposed HTPMM and the prototype. It can be observed that substituting some NdFeB with ferrite can significantly reduce the raw material costs. Ensuring an equivalent NdFeB volume, the cost of permanent magnet materials for the PMC-HTPMM and SMC-HTPMM is 67% and 71%

of that of the prototype, respectively, while maintaining a comparable output performance. This aspect proves advantageous for industrial production.

Table 8. Cost analysis.

	Ferrite Volume (cm^3)	NdFeB Volume (cm^3)	Total Price ($)
Prototype Motor		7.0	4.35
PMC-HTPMM	23.5	3.8	2.9
SMC-HTPMM	29.2	3.8	3.1

4. Electromagnetic Performance Comparison

4.1. No-Load Electromagnetic Characteristics

Considering the rated condition of 1000 rpm for the two hybrid permanent magnet motors and the prototype, the no-load back electromotive force waveforms are depicted in Figure 13a. Both the newly proposed hybrid rare-earth-free permanent magnet motors exhibit higher amplitudes than the prototype. Furthermore, upon Fourier decomposition, the obtained spectra, as shown in Figure 13b, reveal that the SMC-HTPMM has the highest fundamental amplitude. However, it contains more of the seventh harmonic. Conversely, the PMC-HTPMM exhibits more fifth and seventh harmonics. Notably, the prototype motor showcases the highest fifth harmonic content. The no-load back electromotive force is an important parameter characterizing motor performance. The reduction in harmonic content is advantageous for lowering the motor losses, enhancing the motor efficiency, and mitigating the torque ripple, mechanical vibrations, and electromagnetic noise during motor operation, thereby contributing to smoother motor operation. Figure 14 illustrates the air-gap flux density of the three motors, indicating that both the PMC-HTPMM and SMC-HTPMM have higher fundamental air-gap flux density values than the prototype. It is observed that the PMC-HTPMM exhibits more third harmonics, while the SMC-HTPMM has a lower harmonic content compared to the other two motors.

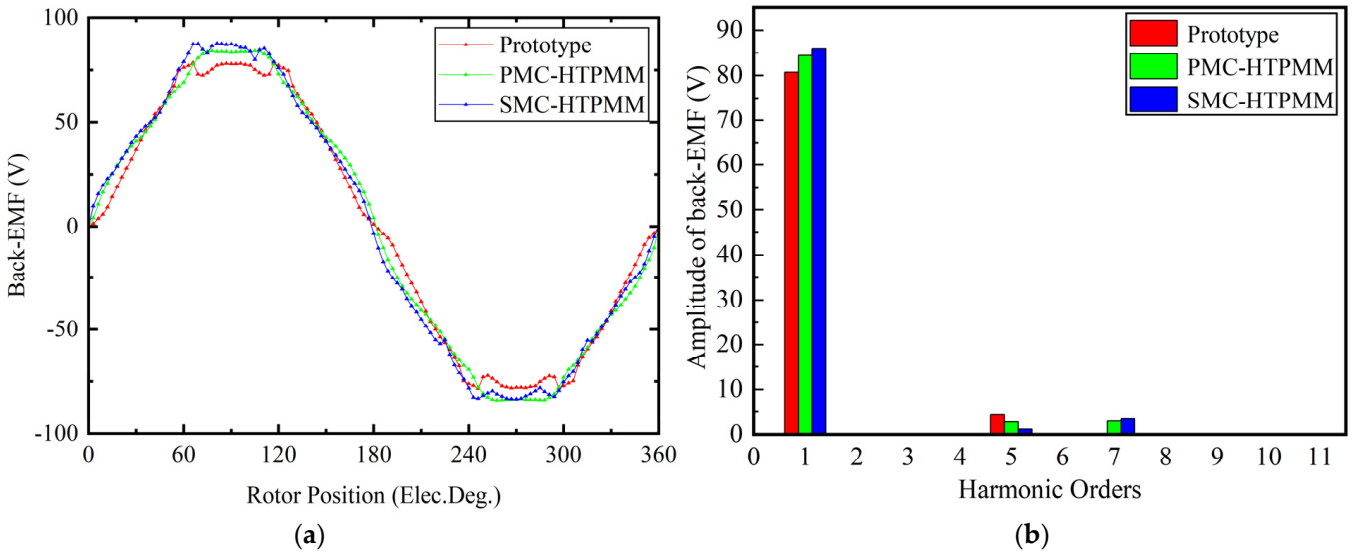

Figure 13. Comparison of no-load back electromotive force: (**a**) no-load back electromotive force; (**b**) spectrum.

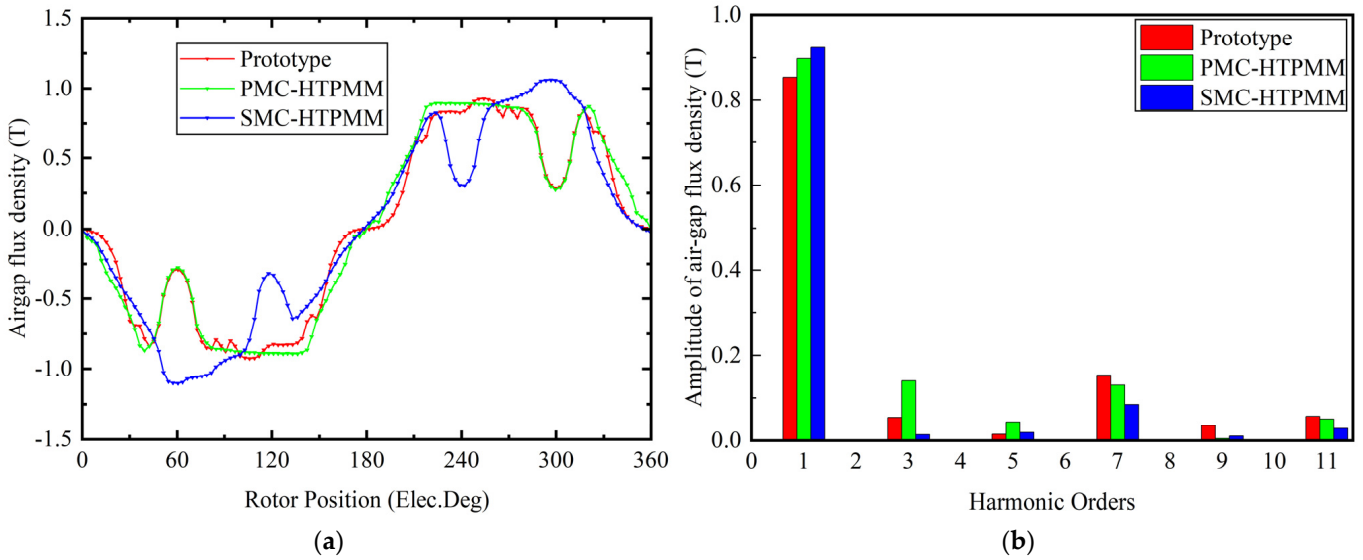

Figure 14. Comparison of no-load air-gap flux density: (**a**) air-gap flux density; (**b**) spectrum.

4.2. Loaded Electromagnetic Characteristics

At a speed of 1000 rpm and with a phase current of 5 A during motor winding, the electromagnetic torque of the three motors is depicted in Figure 15a. The maximum torque of the SMC-HTPMM surpasses those of the other two motors. However, as shown in Figure 15b, the PMC-HTPMM and the prototype exhibit similar motor performances. Due to the influence of magnetic saturation in the magnetic bridge, the load performance of the PMC-HTPMM has a significantly higher torque ripple. Compared to the prototype motors' torque ripple of 8.4%, the PMC-HTPMM's torque ripple reaches 15%.

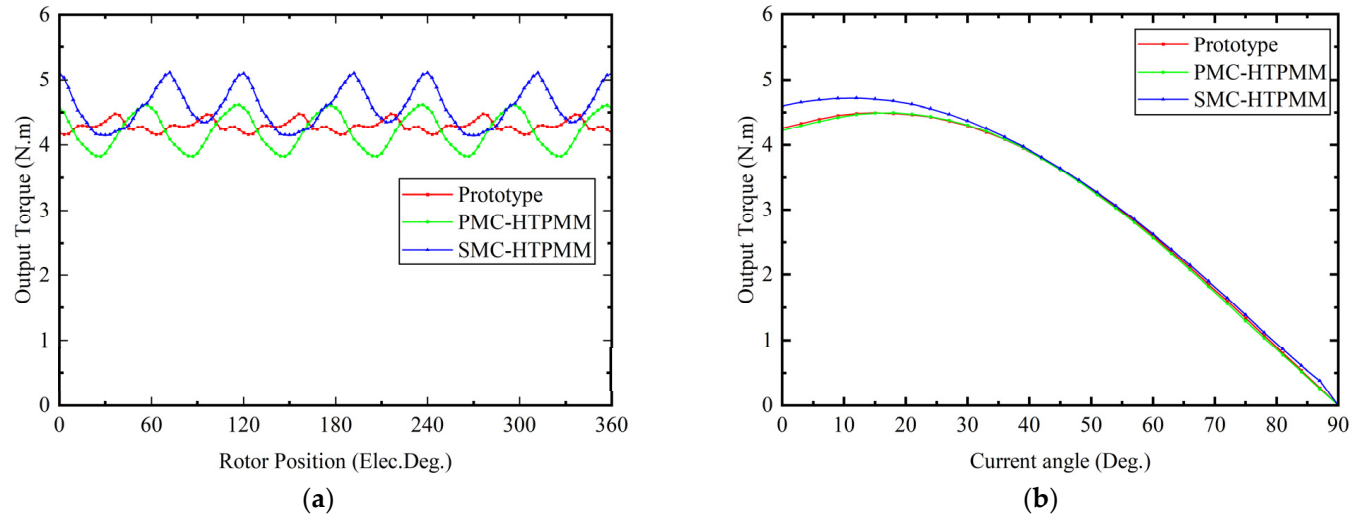

Figure 15. Output torque: (**a**) maximum torque; (**b**) different current phase angles.

4.3. Demagnetization Characteristics

The temperature and armature current are the primary factors influencing magnet demagnetization; temperature fluctuations alter the demagnetization resistance of permanent magnetic materials, while changes in armature current directly impact the demagnetization magnetic field strength. In this section, the demagnetization analysis of the PMC-HTPMM and SMC-HTPMM is conducted using finite element software. The concept of the Demag-

netization Ratio (D_r) is introduced in this work as a quantifiable measure to assess the degree of demagnetization. Subsequently, Equation (1) denotes the formula for D_r.

$$D_r = \left(1 - \frac{Br}{Br_{org}(T)}\right) \times 100\% \quad (1)$$

here, Br denotes the residual magnetic flux density at that specific time point, Br_{org} signifies the residual magnetic flux density without demagnetization, and T stands for the temperature at that moment. We conduct the demagnetization analysis of two hybrid permanent magnet motors at below 1.5 times the rated load. Figure 16 illustrates the demagnetization statuses of the ferrite and NdFeB permanent magnets when a demagnetizing current of 7.5 A is supplied during motor winding. Both the ferrite and NdFeB temperatures were maintained at 100 °C.

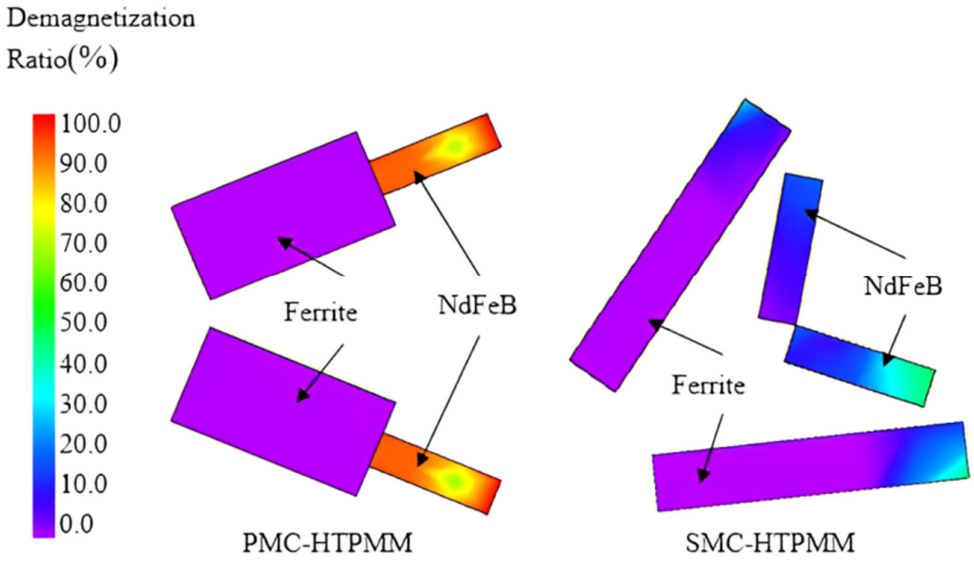

Figure 16. Demagnetization characteristics.

The graph highlights that in the PMC-HTPMM, the demagnetization rate of NdFeB is notably higher, whereas the demagnetization of ferrite is less prominent due to minimal influence from the armature magnetic field. In the SMC-HTPMM, slight demagnetization is observed in the ferrite near the air-gap end. Meanwhile, the NdFeB in the SMC-HTPMM exhibits a considerably lower demagnetization rate compared to that of NdFeB in the PMC-HTPMM. As a result, it can be concluded that the series magnetic circuit hybrid permanent magnet motor demonstrates a superior resistance to demagnetization in comparison to the parallel magnetic circuit hybrid motor.

5. Conclusions

In essence, our study aims to reduce the motor manufacturing costs by introducing two different rotor models for hybrid permanent magnet motors—series and parallel magnetic circuits. Using equal volumes of rare earth permanent magnet materials, we unveil various. performance differences compared to the prototype.

The HTPMM with a parallel magnetic circuit demonstrates a comparable output performance to the prototype in terms of the no-load back EMF, harmonic content, and average torque. Conversely, the hybrid permanent magnet motor with a series magnetic circuit, despite a slight increase in the fundamental amplitude of no-load back electromotive force and air-gap magnetic flux density, exhibits a superior excitation torque, resulting in the highest output torque among the three motors. Additionally, the newly proposed HTPMM presents a significant cost advantage in terms of the permanent magnet material costs, with PMC-HTPMMs material cost being 67% and SMC-HTPMMs being 71% of that of

the prototype. However, the complex rotor topology may introduce additional production steps, necessitating the comprehensive consideration of this factor.

Of note, the study emphasizes the impact of THD of the no-load back electromotive force on motor excitation torque, establishing a trend between the THD and peak-to-peak values of no-load torque. The analysis of demagnetization resistance indicates that, in the parallel magnetic circuit motors, the extensive irreversible demagnetization of NdFeB occurs, while in the series magnetic circuit motors, less irreversible demagnetization occurs. Therefore, compared to the parallel magnetic circuit structure, the series magnetic circuit structure exhibits a lower demagnetization risk.

Looking ahead, detailed experimental results, particularly those related to prototype manufacturing, motor efficiency, and vibration noise, will be presented in future articles to provide a comprehensive understanding of the impact of these hybrid permanent magnet motors on motor manufacturing efficiency and performance optimization.

Author Contributions: Conceptualization; funding acquisition; supervision; verification; and writing—review and editing, L.Z. Methodology; formal analysis; and writing—original draft, K.Y. Software and investigation, M.W. and C.D. All authors have read and agreed to the published version of the manuscript.

Funding: This research was funded by the National Natural Science Foundation of China 52077042.

Data Availability Statement: Data are contained within the article.

Conflicts of Interest: The authors declare no conflicts of interest.

References

1. Roboam, X. A Review of Powertrain Electrification for Greener Aircraft. *Energies* **2023**, *16*, 6831. [CrossRef]
2. Li, X.; Yu, S.; Wang, Y. A Novel HTS Claw-Pole Vernier Machine Using Single Excitation Unit with Stationary Seal. *IEEE Trans. Appl. Supercond.* **2019**, *29*, 1–5. [CrossRef]
3. Chen, Q.; Xu, G.; Zhai, F.; Liu, G. A Novel Spoke-Type PM Motor with Auxiliary Salient Poles for Low Torque Pulsation. *IEEE Trans. Ind. Electron.* **2020**, *67*, 4762–4773. [CrossRef]
4. Yang, H.; Zhu, Z.Q.; Lin, H.; Chu, W. Flux Adjustable Permanent Magnet Machines: A Technology Status Review. *Chin. J. Electr. Eng.* **2016**, *2*, 14–30.
5. US Department of Energy. Advanced Vehicle Technologies Research Funding Opportunity Announcement. 2020. Available online: https://www.energy.gov/eere/vehicles/funding-opportunities (accessed on 7 January 2024).
6. Hua, H.; Zhu, Z.Q.; Wang, C.; Zheng, M.; Wu, Z.; Wu, D.; Ge, X. Partitioned Stator Machines with NdFeB and Ferrite Magnets. *IEEE Trans. Ind. Appl.* **2017**, *53*, 1870–1882. [CrossRef]
7. Boldea, I.; Tutelea, L.N.; Parsa, L.; Dorrell, D. Automotive Electric Propulsion Systems with Reduced or No Permanent Magnets: An Overview. *IEEE Trans. Ind. Electron.* **2014**, *61*, 5696–5711. [CrossRef]
8. Galioto, S.J.; Reddy, P.B.; EL-Refaie, A.M.; Alexander, J.P. Effect of Magnet Types on Performance of High-Speed Spoke Interior-Permanent-Magnet Machines Designed for Traction Applications. *IEEE Trans. Ind. Appl.* **2015**, *51*, 2148–2160. [CrossRef]
9. McFarland, J.D.; Jahns, T.M.; EL-Refaie, A.M.; Reddy, P.B. Effect of Magnet Properties on Power Density and Flux-Weakening Performance of High-Speed Interior Permanent Magnet Synchronous Machines. In Proceedings of the 2014 IEEE Energy Conversion Congress and Exposition (ECCE), Pittsburgh, PA, USA, 14–18 September 2014; pp. 4218–4225.
10. Wu, W.; Zhu, X.; Quan, L.; Fan, D.; Xiang, Z. Characteristic Analysis of a Less-Rare-Earth Hybrid PM-Assisted Synchronous Reluctance Motor for EVs Application. *AIP Adv.* **2017**, *7*, 056648. [CrossRef]
11. Poudel, B.; Amiri, E.; Rastgoufard, P.; Mirafzal, B. Toward Less Rare-Earth Permanent Magnet in Electric Machines: A Review. *IEEE Trans. Magn.* **2021**, *57*, 900119. [CrossRef]
12. Yunyun, C.; Tongle, C.; Xiaoyong, Z.; Yu, D. Optimization of a New Asymmetric-Hybrid Machine with High Torque Density and Low Torque Ripple Considering the Difference of Magnetic Materials. *IEEE Trans. Magn.* **2022**, *58*, 1–5. [CrossRef]
13. Afinowi, I.A.A.; Zhu, Z.Q.; Guan, Y.; Mipo, J.-C.; Farah, P. Switched-Flux Machines with Hybrid NdFeB and Ferrite Magnets. *COMPEL Int. J. Comput. Math. Electr. Electron. Eng.* **2016**, *35*, 456–472. [CrossRef]
14. Wang, M.; Tong, C.; Zheng, P.; Cheng, L.; Zhang, S.; Qiao, G.; Sui, Y. Analysis of a Novel Hybrid Variable-Flux Machine Using New Magnet Material CeFeB. *IEEE Trans. Magn.* **2019**, *55*, 1–7. [CrossRef]
15. Zeng, X.; Quan, L.; Zhu, X.; Xu, L.; Liu, F. Investigation of an Asymmetrical Rotor Hybrid Permanent Magnet Motor for Approaching Maximum Output Torque. *IEEE Trans. Appl. Supercond.* **2019**, *29*, 1–4. [CrossRef]
16. Zhu, X.; Fan, D.; Xiang, Z.; Quan, L.; Hua, W.; Cheng, M. Systematic Multi-Level Optimization Design and Dynamic Control of Less-Rare-Earth Hybrid Permanent Magnet Motor for All-Climatic Electric Vehicles. *Appl. Energy* **2019**, *253*, 113549. [CrossRef]

17. Chen, Q.; Liu, G.; Zhao, W.; Shao, M.; Liu, Z. Design and Analysis of the New High-Reliability Motors with Hybrid Permanent Magnet Material. *IEEE Trans. Magn.* **2014**, *50*, 1–10. [CrossRef]
18. Du, Z.S.; Lipo, T.A. Interior Permanent Magnet Machines with Rare Earth and Ferrite Permanent Magnets. In Proceedings of the 2017 IEEE International Electric Machines and Drives Conference (IEMDC), Miami, FL, USA, 21–24 May 2017; pp. 1–8.
19. Du, Z.S.; Lipo, T.A. Cost-Effective High Torque Density Bi-Magnet Machines Utilizing Rare Earth and Ferrite Permanent Magnets. *IEEE Trans. Energy Convers.* **2020**, *35*, 1577–1584. [CrossRef]
20. Cai, H.; Guan, B.; Xu, L. Low-Cost Ferrite PM-Assisted Synchronous Reluctance Machine for Electric Vehicles. *IEEE Trans. Ind. Electron.* **2014**, *61*, 5741–5748. [CrossRef]
21. Ma, Q.; El-Refaie, A.; Lequesne, B. Low-Cost Interior Permanent Magnet Machine with Multiple Magnet Types. *IEEE Trans. Ind. Appl.* **2020**, *56*, 1452–1463. [CrossRef]
22. Park, J.; Tsunata, R.; Takemoto, M.; Orikawa, K.; Ogasawara, S. Investigation of Dy-Free Hybrid PM Motor Based on Spoke-Type Rotor for Automotive Applications. In Proceedings of the 2021 IEEE International Electric Machines & Drives Conference (IEMDC), Hartford, CT, USA, 17–20 May 2021; pp. 1–8.